

Potential involvement of chemicals in liver cancer progression: An alternative toxicological approach combining biomarkers and innovative technologies



Ludovic Peyre^{a,*}, Nathalie Zucchini-Pascal^a, Georges de Sousa^a, Anne-Pascale Luzy^b, Roger Rahmani^{a,*}

^aUMR 1331 TOXALIM (Research Centre in Food Toxicology), Institut National de la Recherche Agronomique (INRA), Laboratory of Xenobiotics Cellular and Molecular Toxicology, 400 route des Chappes, BP 167, 06903 Sophia-Antipolis Cedex, France

^bGALDERMA R&D, Early Admet, 06902 Sophia Antipolis, France

ARTICLE INFO

Article history:

Received 11 February 2014

Accepted 23 June 2014

Available online 2 July 2014

Keywords:

Real-time cellular impedance

High content screening

Epithelial–mesenchymal transition

Hepatic homeostasis dysregulation

Cancer

Environmental pollutants

ABSTRACT

Pesticides as well as many other environmental pollutants are considered as risk factors for the initiation and the progression of cancer. In order to evaluate the *in vitro* effects of chemicals present in the diet, we began by combining viability, real-time cellular impedance and high throughput screening data to identify a concentration “zone of interest” for the six xenobiotics selected: endosulfan, dioxin, carbaryl, carbendazim, p,p'DDE and hydroquinone. We identified a single concentration of each pollutant allowing a modulation of the impedance in the absence of vital changes (nuclear integrity, mitochondrial membrane potential, cell death). Based on the number of observed modulations known to be involved in hepatic homeostasis dysfunction that may lead to cancer progression such as cell cycle and apoptosis regulators, EMT biomarkers and signal transduction pathways, we then ranked the pollutants in terms of their toxicity. Endosulfan, was able to strongly modulate all the studied cellular processes in HepG2 cells, followed by dioxin, then carbendazim. While p,p'DDE, carbaryl and hydroquinone seemed to affect fewer functions, their effects nevertheless warrant close scrutiny. Our *in vitro* data indicate that these xenobiotics may contribute to the evolution and worsening of hepatocarcinoma, whether via the induction of the EMT process and/or via the deregulation of liver key processes such as cell cycle and resistance to apoptosis.

© 2014 Elsevier Ltd. All rights reserved.

1. Introduction

To ensure the safety of new molecules on human health and the environment, both public and private institutions have in recent years greatly promoted the development of alternative methods in toxicology to replace animal experiments deemed both unethical and not always representative of xenobiotic effects in humans (Olson et al., 2000). Current regulations for compound approval require manufacturers to perform numerous tests, many of which use liver cells as toxicological model. Indeed, the liver is the main organ of detoxification within the human body and is where xenobiotics are metabolized prior to their excretion. In addition to being long and costly, such regulatory measures could also be considered

as insufficient in light of several molecules being withdrawn from market following suspicions raised by healthcare professionals and pressure from the governments concerned. Indeed, many environmental contaminants including drugs and pesticides have now been recognized as risk factors for hepatic diseases (Mostafalou and Abdollahi, 2013) that affect not only farmers and workers within the agrochemical industry but the entire population (Ferris et al., 2008). Yet, although epidemiologic studies tend to highlight the statistically relevant link between chemicals and hepatocarcinoma (HCC), the molecular mechanisms remain unclear. Our vision of a single molecular pathway is insufficient and should instead incorporate many pathways combined that relate to other perturbations of cellular homeostasis such as apoptosis, cell cycle dysregulation, or epithelial to mesenchymal transition (EMT), three processes involved in carcinoma progression and leading to metastasis (Fabregat, 2009).

The EMT process is complex and comprises a succession of events leading to the loss of epithelial characteristics. This phenomenon can be studied by monitoring the disappearance of

* Corresponding authors. Address: Laboratoire de Toxicologie Cellulaire, Moléculaire des xénobiotiques, INRA, UMR 1331, 400 route des Chappes, BP167, 06903 Sophia Antipolis, France. Tel.: +33 4 92 38 65 48; fax: +33 4 92 38 64 01.

E-mail addresses: ludovic.peyre@sophia.inra.fr (L. Peyre), Roger.rahmani@sophia.inra.fr (R. Rahmani).

specific markers, particularly in the dissociation of adherent junctions in which E-cadherin is downregulated by the modulation of expression of many transcription factors such as Snail or Slug known to be controlled by different pathways including TGF- β /Smad, (Dang et al., 2011). This step induces the stabilization of β -catenin protein and the activation of the Wnt/ β -catenin pathway (Nambotin et al., 2012). In parallel, the increase of mesenchymal markers (fibronectin, S100a4...) is associated with the gain of migratory and invasive properties. It requires two levels of interaction: firstly between the cell and the ECM, and secondly between the same cell and its neighbors (Yang et al., 2011). The contact between cells and the ECM allows the activation of the ERK pathway and the master survival AKT pathway under the control of Fak and ILK respectively (Fuchs et al., 2008). The breakdown of epithelial cell adhesion during EMT is followed by the activation of a survival program (Fabregat et al., 2007). Two potential markers are the anti-apoptotic protein XIAP which has recently been shown to be overexpressed in HCC, and Cyclin D1 which, when coexpressed with XIAP, relates to poor prognosis (Che et al., 2012). On the other hand mesenchymal resistant cancer cells show increased levels of AKT and STAT3 activation (Ji and Wang, 2012), thus highlighting two more potential markers. The consequential inhibition of apoptosis also requires the intervention of survival pathways such as PI3 K/AKT and RAS/ERK pathways described above. Finally, P21^{waf1} was used here as key marker of the cell cycle control in HCC. It acts as a tumor suppressor by inhibiting cyclin complexes but can also exhibit oncogenic activities in certain contexts (Buitrago-Molina et al., 2013).

In our laboratory, we have recently developed the technology of High Content Screening (HCS) which combines in one device the simultaneous measurements performed by fluorescence microscopy, flow cytometry and microplate reader. Interestingly, all data collected can be processed via a simultaneous high-throughput analysis. This innovative and multi-functional "Cytomic" technology analyses live cells responding to chemical stress by combining assessments of such as proliferation, apoptosis, metabolism, morphology or signaling pathways (O'Brien et al., 2006; Tolosa et al., 2012). In parallel we use the xCELLigence system to measure real-time changes in electrical impedance of culture cells across microelectrodes integrated into the bottom of a 96-well plate. The cell status is then quantified and annotated as a Cell Index (CI), according to a specific equation provided by the manufacturer (Ke et al., 2011). In practice and reflecting uniform physiological conditions, more cells attaching onto the electrodes lead to a larger value for the cell index. Furthermore, for the same number of cells per well, a change in the cell status such as morphology, receptor activation or adhesion will lead to a change in the cell index (Atienza et al., 2006).

We selected for this study 6 environmental contaminants still found in water and/or food of the French population despite their prohibition (EAT2, ANSES, 2011). These were dioxin (TCDD) which is considered as a persistent organic pollutant (POP) and as a carcinogen (group 1 CIRC), the two organochlorine pesticides endosulfan and the DDT metabolite p,p'DDE, the two carbamates carbaryl and carbendazim developed in parallel of the ban of organochlorines, and finally hydroquinone which is used in several industries including pharmaceutical, cosmetics and agrochemical. The hepatocarcinoma cells HepG2 were chosen for their epithelial characteristics and their ability to acquire metastatic behavior in response to certain agents (Zucchini-Pascal et al., 2013).

The aim of this work was to evaluate *in vitro* the six xenobiotics selected using real-time cellular impedance and HCS technologies combined with EMT and HCC biomarkers, in order to provide new evidence for an effect of these chemicals on liver cancer progression that may lead to metastasis.

2. Materials and methods

2.1. Materials

The human hepatocellular carcinoma cell line HepG2 was obtained from ATCC (American Type Culture Collection, Manassas, VA). Dulbecco's modified Eagle's medium (DMEM), fetal bovine serum (FBS), penicillin–streptomycin solution, sodium pyruvate and Eagle's non-essential amino acids were from BioWhittaker (Cambrex company, Walkersville, MD, USA). Dimethylsulfoxide (DMSO), endosulfan, carbaryl, carbendazim and hydroquinone were from Sigma–Aldrich (L'Isle d'Abeau Chesne, Saint Quentin Fallavier, France), p,p'DDE from Chem Service (West Chester, USA) and TCDD from AccuStandard, USA. Protein assay materials were from Bio-Rad, Hoechst 33342 and TMRE from Molecular Probes (Eugene, OR) and the antibodies used for western blotting experiments from Cell Signaling, Epitomics and Neomarkers (Table 1).

2.2. Cell culture and chemical treatments

HepG2 cells were maintained in DMEM with 1% penicillin/streptomycin, 1% nonessential amino acids, 1% sodium pyruvate and 10% FBS, in humidified atmosphere at 37 °C containing 95% O₂ and 5% CO₂. After washing with sterile phosphate buffer saline (PBS), cells were detached by trypsinization (trypsin/EDTA) and, depending on the experiment, plated at a concentration of 0.5–2 × 10⁶ cells in 6-well plates or 1 × 10⁴ in 96-well plates. For all experimental conditions, FBS was reduced to 5% in DMEM medium. The mitogen-activated protein kinase (MEK) 1/2 inhibitor U0126 was added at a concentration of 5 μM and the control cyclosporine A was used at 30 μM. All chemicals and pharmacological inhibitors were prepared as stock solutions in DMSO. The final concentration of DMSO in the medium was 0.25% in all conditions.

2.3. Viability test

Viable cells were determined by measuring the conversion of the tetrazolium salt MTT 3-(4,5-dimethylthiazol-2-yl)-2,5-diphenyltetrazolium bromide, Sigma–Aldrich (St. Louis, MO) to formazan, as previously described (Fautrel et al., 1991). Briefly, cells were seeded in 96-well plates and treated at 50% confluency with a concentration of 20 μM endosulfan during 48 h. The cells were

Table 1
Primary antibodies used for western blot.

Antigen	Phosphorylation site	Source/type	Manufacturer	Dilution
pErk1/2	thr202/tyr204	Rabbit mAb1	Cell signaling	1:2000
Erk2		Rabbit pAb2	Cell signaling	1:5000
pAkt	Thr308	Rabbit pAb	Cell signaling	1:2000
Akt		Rabbit pAb	Cell signaling	1:2000
pSmad1/5	Ser463/465	Rabbit mAb	Cell signaling	1:2000
pSmad2	Ser465/467	Rabbit mAb	Cell signaling	1:2000
Smad5		Rabbit pAb	Cell signaling	1:2000
pStat3	Tyr705	Rabbit pAb	Cell signaling	1:2000
Cyclin D1		Rabbit pAb	NeoMarkers	1:2000
P21waf1		Rabbit mAb	NeoMarkers	1:2000
Bax		Rabbit pAb	Cell signaling	1:2000
Bcl-xl		Rabbit mAb	Cell signaling	1:2000
pFak	Tyr925	Rabbit pAb	Cell signaling	1:2000
Fak		Rabbit pAb	Cell signaling	1:2000
Gapdh		Rabbit mAb	Cell signaling	1:15000
E-cadherin		Rabbit mAb	Epitomics	1:5000
β -catenin		Mouse mAb	Santa Cruz	1:2000
Fibronectin		Rabbit mAb	Epitomics	1:1000
Snail1		Rabbit pAb	Santa Cruz	1:1000

1: mAb. monoclonal antibody.

2: pAb. polyclonal antibody.

then incubated with 0.5 mg/ml MTT for 2 h at 37 °C. The water-insoluble formazan crystal was dissolved by adding 100 µl DMSO to each well and the absorbance was determined with a spectrophotometer at 550 nm (MR7000, Dynatech Laboratories, Inc., USA).

2.4. Real-time reverse transcription-polymerase chain reaction

Total RNA was isolated using Trizol extraction. One microgram of total RNA was reverse transcribed using SuperScript II (Invitrogen Corp, Carlsbad, California) following the manufacturer's instructions. The resulting complementary DNA was diluted 100-fold and for each gene (target genes *CCND1*, *CDH1*, *FN1*, *FSP1*, *ILK*, *P21^{waf1}*, *XIAP* or reference gene *GAPDH*) and each condition, a mixture of Taq polymerase, 6.4 mmol/L of magnesium chloride, deoxynucleotide triphosphate, primer, and probe (<https://www.rocke-applied-science.com>) was added. The cDNA was then amplified in a thermocycler (LightCycler 480; Roche Applied Science, Penzberg, Upper Bavaria, Germany) for 45 cycles using conditions of 95 °C and 60 °C for 10 s each. Commercially available software (LightCycler 480; Roche Applied Science) was used for relative quantitative analysis.

2.5. Western blot

Cells were scraped into hypotonic buffer (20 mM HEPES pH7.5, 10 mM KCl, 15 mM MgCl₂, 0.25 mM sucrose, 1 mM EDTA, 1 mM EGTA, 1 mM DTT, 0.1 mM PMSF, 10 µg/ml pepstatin A, 10 µg/ml leupeptin, and the phosphatase inhibitory cocktail PhosphoSTOP, Roche). The protein concentration in each cell lysate was measured with a BCA Protein Assay Kit (Pierce), using bovine serum albumin (BSA) as a standard. Equal protein amounts were separated by SDS-polyacrylamide gel electrophoresis on 10% or 12% gels and were transferred to PVDF membranes. The membranes were immunoblotted with antibodies (cf. Table 1 for names, origins and concentrations) for 1 h at room temperature or overnight at 4 °C. The membranes were then incubated with horseradish peroxidase-conjugated secondary antibodies (anti-mouse or anti-rabbit immunoglobulin G; Promega, Madison, WI, USA) for 2 h at room temperature. After washing, an ECL detection kit was used to react with the secondary antibodies. The signal was acquired with a CDD camera (ChemiGenius2, Syngene) and semi-quantitative analysis was then carried out with GeneTools software.

2.6. Real-time cellular impedance

The xCELLigence® system was used according to the manufacturers' instructions (Roche Applied Science, Mannheim, Germany) and ACEA Biosciences (San Diego, CA, USA). Briefly, 1×10^4 cells/well were added to the 96-well E-plates before being treated 24 h later with chemicals and/or pharmacological inhibitors in a DMEM medium supplemented with 10% of FBS. Real-time cellular impedance is measured in each well (Cell Index values) and the signal observed via the integrated software (RTCA analyzer). To observe the influence of chemicals on cells in comparison with the DMSO control, the Normalized Cell Index (NCI_{ti}) based on the last time point before compound addition was used. Each curve is representative of one experiment performed at least in triplicate (technical replicates). Data represent the average ± standard deviation of one of three independent and reproducible experiments as described previously (Atienzar et al., 2011).

2.7. Cell imaging microplate assays and cellomics ArrayScanXTI scanning details

HepG2 cells were seeded at 10,000 cells per well in black 96-well cell culture plates and allowed to attach overnight in the

incubator. 24 h later, the tetramethylrhodamine ethyl ester perchlorate TMRE (Molecular Probes) was used following the recommendations of the manufacturer in order to detect variations of the mitochondrial membrane potential sequestered by active mitochondria. Briefly, cells were treated for 24 h with different concentrations of xenobiotics. Then the stock concentration (2.4 mM) of TMRE contained in DMSO was diluted in a serum and red phenol free medium. 100 µl of the final solution (25 nM) was added per well and incubated during 30 min with the nuclear marker Hoechst 33342 (2.5 µg/ml final) at 37 °C. After two steps of washing with PBS buffer, cells were fixed with 3.7% paraformaldehyde during 10 min at 37 °C. Plates were washed again twice before being scanned with the ArrayScanXTI instrument (Cellomics Inc., Pittsburgh, USA). The mitochondrial membrane potential detection and the nuclear Area calculation were performed with the "compartmental analysis" bio-application, and the cell cycle modulation in response to xenobiotics was calculated with the "Cell Cycle" bio-application (Cellomics Inc., Pittsburgh, USA). The number of cells to analyze was fixed between 500 and 2000 per well depending on the bio-application. An objective of 20X was used for imaging analysis. The nuclear dye (Hoechst) was detected in channel 1 (excitation filter 386 nm). The 'objects' targeted to measure in channels 2, were defined by expanding the circular region of the nuclei to include the cytoplasm of the cell. Channel 2 (filter set 549/600 nm) was used to detect the TMRE. The Cellomics ArrayScanXTI output feature "mean ring spot total intensity" was used to analyze the scans. For each plate, the average of the 3 control wells (0.25% DMSO) was used as a reference level and rescaled to 1. Each well value was expressed relative to this reference value. A value of 2 meant a 2-fold induction of the fluorescent signal compared to the control value.

2.8. Enzymatic assays for caspase activity

Caspase activity was assessed by measuring fluorophore (7-amido-4-trifluoromethylcoumarin (AFC)) release from caspase tetrapeptide substrate *N*-acetyl-Asp-Glu-Val-Asp (Ac-DEVD) for caspase-3-like activity. Briefly, cells grown in 6-well culture dishes were scraped into ice-cold hypotonic buffer. Cells were lysed by being subjected to three cycles of freezing and thawing. Protein concentrations were determined using the BCA Protein Assay kit (Pierce, Rockford, IL, USA) and equal amounts were mixed with buffer B (312.5 mM HEPES, pH 7.5, 31.25% sucrose, 0.3125% CHAPS, and 50 M of relative substrate enzymes). The fluorometric assay detects the shift in AFC fluorescence emission following cleavage from tetrapeptide-AFC, as measured in a fluorometer (ex = 390 nm; em = 530 nm).

2.9. Statistical analysis

Each experiment was repeated at least three times. Data shown are an average ± standard deviation (SD). Statistical analysis of *in vitro* studies was performed using a Student's *t* test. Levels of probability are indicated: **P* < 0.05 or ***P* < 0.01

3. Results

3.1. Combining MTT test and real-time cellular Impedance to predict HepG2 cell viability

In order to select a subtoxic concentration zone for each xenobiotic used, we first tested 7 concentrations per compound using real-time cellular impedance in parallel with the MTT assay at 48 h, the maximum time at which we performed experiments. As shown in Fig. 1A and B, the MTT test seemed to be more sensitive

with regards evaluating cell viability with endosulfan. Indeed, while the MTT test revealed decreases of 20% and 70% cell viability at 50 and 100 μM respectively, the xCELLigence system suggested a reduction of only 20% for 100 μM of endosulfan. This decrease in viability could have been masked by the increase in the Normalized Cell Index (NCI) induced by the organochloride pesticide, a phenomenon that can be observed between 0.1 and 20 μM . At these concentrations, no changes were observed with the MTT test in terms of proliferation or death process, suggesting a possible modification in cell morphology. Based on this analysis model (no toxicity, no proliferation but changes in NCI), we made the same investigation with the other 5 pollutants. As shown in Fig. 1C and D, we noted a decrease in NCI at 100 and 500 μM carbaryl that corresponded to a decrease in the cell viability revealed by MTT assay. This test allowed us to observe that compared to the control DMSO, 500 μM of carbaryl was also prejudicial with a loss of about 50% of viability whereas no differences were observed on the xCELLigence system. However, an increase in the NCI at 48 h for doses between 1 and 100 μM was observed. We then studied the effects of carbendazim on viability as shown in Fig. 2A and B. Real-time cellular impedance analysis revealed a strong increase in NCI for concentrations between 0.1 and 5 μM , and inversely a decrease between 10 and 125 μM . This corresponds to the decrease in cell viability that is already detectable from 5 μM using MTT assay. As shown in Fig. 2B and C, a clear pattern emerged from the p,p'DDE treatment. MTT and xCELLigence curves were quite similar, showing an increase in viability and NCI at low doses of

2.5–25 μM and a decrease at higher concentrations between 125 μM and 1.25 mM. As shown in Fig. 3A and B, no significant modulation of the NCI was found at 48 h for hydroquinone concentrations between 1 and 100 μM . A transient decrease in NCI occurred at 250 μM during the first 24 h before stabilizing at 48 h, with greater decreases occurring at 500 μM and 1 mM. This observation was supported by the MTT assay which displayed a decrease at 100 μM , a lower concentration than that causing a decrease detectable via real-time cellular impedance. Finally, performing the same tests on dioxin (TCDD) revealed its non-toxicity at concentrations between 6 nM and 48 nM. Cell viability did however decrease at concentrations between 97 and 397 nM. Interestingly, we noticed a strong increase in the NCI in response to TCDD with a maximum at concentrations between 12 and 48 nM.

3.2. HCS to complement the viability data

To complete the above data and to select a relevant concentration of each molecule for further study, we decided to assess different factors that could indicate toxicity (Tolosa et al., 2012; Xu et al., 2008). For this experiment, the two high and toxic doses were removed. Firstly, we used HCS technology to calculate the average area of the nucleus that has been shown to be reduced in the presence of toxic concentrations. As expected, Hoechst 33342 staining revealed a decrease of the nuclear area at 24 h for 100 and 500 μM carbaryl, 125 and 250 μM p,p'DDE, 50 μM endosulfan and 250 μM hydroquinone (Fig. 4A). We then used the ArrayScan cell cycle

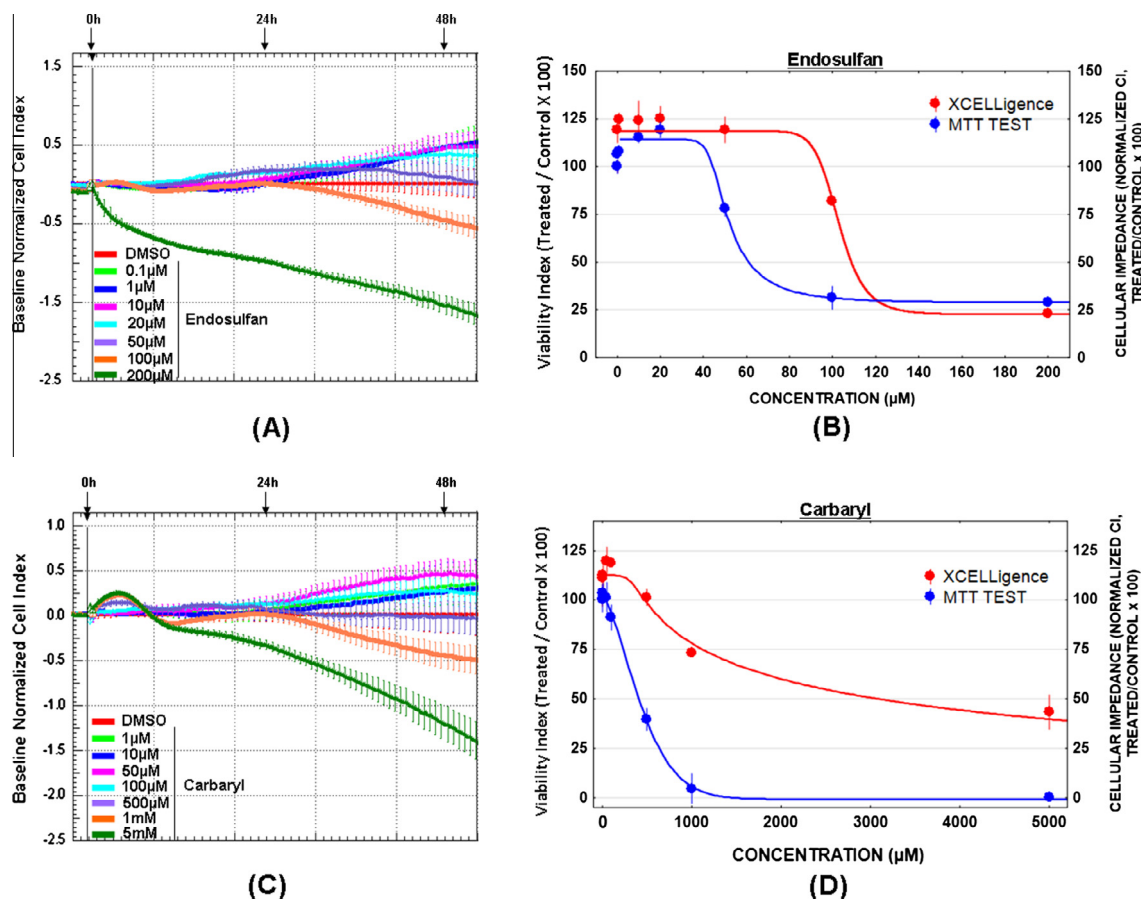


Fig. 1. Comparison between MTT test and real-time cellular impedance to predict HepG2 cell viability. (A and C) Cells were seeded onto 96-well E-plates and treated for at least 48 h with endosulfan (from 0.1 μM to 200 μM) or carbaryl (from 1 μM to 5 mM). Cell impedance was measured in real-time and cell index normalized against the DMSO condition. Results are means \pm S.D. for triplicates of one experiment and are representative of three independent experiments. (B and D) HepG2 cell viability was assessed by MTT test after 48 h treatment with increasing concentrations of endosulfan (from 0.1 μM to 200 μM) or carbaryl (from 1 μM to 5 mM). MTT results are compared with impedance results at 48 h and presented as a percentage of viability over DMSO treatment and each value is the mean \pm S.D. of three separate experiments.

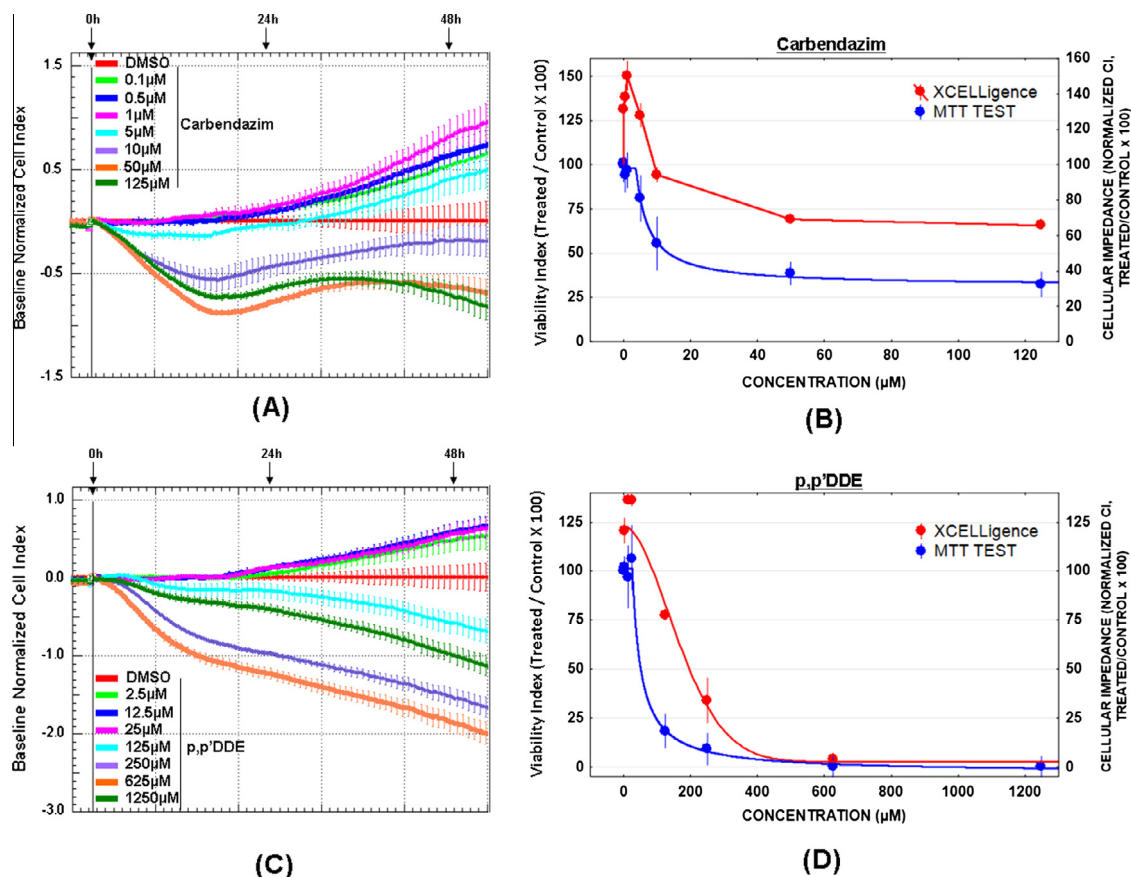


Fig. 2. Comparison between MTT test and real-time cellular impedance to predict HepG2 cell viability. (A and C) Cells were seeded onto 96-well E-plates and treated for at least 48 h with carbendazim (from 0.1 μM to 125 μM) or p,p'DDE (from 2.5 μM to 1.25 mM). Cell impedance was measured in real-time and cell index normalized against the DMSO condition. Results are means \pm S.D. for triplicates of one experiment and are representative of three independent experiments. (B and D) HepG2 cell viability was assessed by MTT test after 48 h treatment with increasing concentrations of carbendazim (from 0.1 μM to 125 μM) or p,p'DDE (from 2.5 μM to 625 μM). MTT results are compared with impedance results at 48 h and presented as a percentage of viability over DMSO treatment and each value is the mean \pm S.D. of three separate experiments.

bio-application (see material and methods) to calculate the percentage of cells below 2 N, i.e. the proportion of cells detected with a lower nuclear DNA content (sub G0/G1 fraction) than the control condition DMSO (Fig. 4B). This provided supplementary information on cell status by highlighting the possible apoptotic or necrotic population. Concordantly, we noticed an increase of the cell population below 2 N after treatments with 100 and 500 μM carbaryl, 125 and 250 μM p,p'DDE, 50 μM endosulfan and 250 μM hydroquinone. However we also observed an increase for 100 μM hydroquinone and 50 μM carbaryl. In parallel, we measured the mitochondrial potential activity of the HepG2 cells after 24 h of treatment (Fig. 4C and D). These data were in agreement by showing a decrease of the mitochondrial activity with 50, 100 and 500 μM carbaryl, 125 and 250 μM p,p'DDE, 50 μM endosulfan and 250 μM hydroquinone. Surprisingly, TCDD seemed to induce a perturbation in mitochondrial activity whatever the concentration tested, with a decrease of 50% at 12, 24 and 48 nM. Combining these preliminary data (Fig. 5), we were able to determine a zone of interest within which we could choose a concentration that neither induced toxicity nor led to major changes in the controls tested (nuclear integrity and mitochondrial activity) and yet caused a change in the NCI. For each molecule, we selected the following relevant concentrations for further evaluation: 20 μM endosulfan, 10 μM carbaryl, 5 μM p,p'DDE and 2.5 μM carbendazim. Exceptions were made for 10 μM hydroquinone which met the criteria of dose selection, i.e. no toxicity and no major changes in major cellular functions but for which we detected no positive response in cell impedance in the range of 1–50 μM , and for

12 nM TCDD which induced as desired an increase in the NCI but with a decrease in mitochondrial activity even at lower doses.

3.3. Effects of the environmental pollutants on cell cycle

Using HCS, we investigated the role of each compound on the cell cycle and its main regulators P21^{waf1} and cyclin D1. In Fig. 6A, we have deliberately kept three concentrations to achieve an overview of the effects of each compound and thus be able to offer a global trend of their effects on the cell cycle. In the control condition DMSO, we observed an average ratio of about 60% of cells in G0/G1 phase, 10% in S phase and 30% in G2/M phase. Treatment with 10 μM carbaryl, 20 μM endosulfan or 10 μM hydroquinone had no significant effect. However, we noted a decrease in the percentage of cells in G0/G1 phase which started at 2.5 μM p,p'DDE and which was significant at 12.5 μM the concentration at which we observed an increase in the G2/M population (40% of cells in G0/G1 and 40% in G2/M). Carbendazim displayed an almost identical profile to p,p'DDE at concentrations of 5–10 μM , yet appeared to have no effect at concentrations of 1–2.5 μM , the lowest concentrations chosen for this experiment. Finally, 12 nM of dioxin induced a decrease in the population of cells in phase G2/M from 30% in the control condition to 20%.

Having chosen and validated a single concentration for each compound of interest through a combination of tools, our investigation then focused on the involvement of the key regulators Cyclin D1 and P21^{waf1} after 48 h of treatment of HepG2 cells. Cyclin D1 is involved in cancer progression and acts as a biomarker of

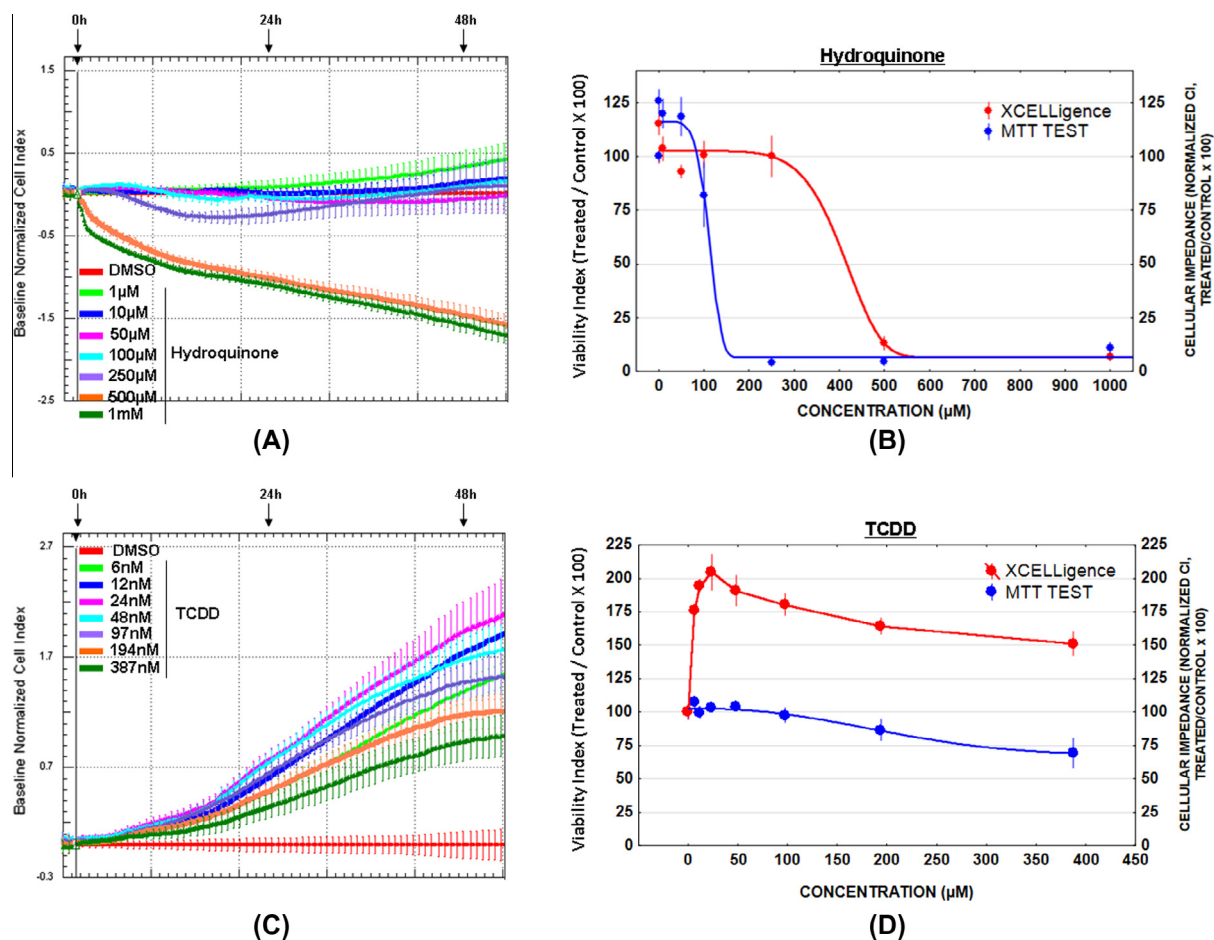


Fig. 3. Comparison between MTT test and real-time cellular impedance to predict HepG2 cell viability. (A and C) Cells were seeded onto 96-well E-plates and treated for at least 48 h with hydroquinone (from 1 μM to 1 mM) or TCDD (from 6 nM to 387 nM). Cell impedance was measured in real-time and cell index normalized to the DMSO condition. Results are means \pm S.D. for triplicates of one experiment and are representative of three independent experiments. (B and D) HepG2 cell viability was assessed by MTT test after 48 h treatment with increasing concentrations of hydroquinone (from 1 μM to 1 mM) or TCDD (from 6 nM to 387 nM). MTT results are compared with impedance results at 48 h and presented as a percentage of viability over DMSO treatment; each value is the mean \pm S.D. of three separate experiments.

cancer prognosis whereas P21 is considered a tumor suppressor due to its role as a key negative regulator of the cell cycle and cell proliferation. Using western blotting (Fig. 6B) and quantitative PCR (Fig. 6C and D), we wished to observe the effects of the 6 xenobiotics on gene and protein expressions. The expression of cyclin D1 at both the gene and protein levels was upregulated with TCDD, endosulfan and p,p'DDE. In parallel, we observed the upregulation of P21^{waf1} gene and protein expression after treatment with endosulfan, p,p'DDE and hydroquinone. TCDD seemed only to affect the expression of P21^{waf1} at the protein level.

3.4. Dysregulation of the apoptotic pathway

This dysregulated balance between survival and apoptosis was shown to occur in liver cancer and partly participate towards progression to HCC. Only TCDD and endosulfan were able to induce Caspase-3 like activity at 4 h; hydroquinone induced it at 48 h (Fig. 7A). To provide evidence to support this observation in terms of apoptotic tendency, we analyzed the ratio Bcl-xl/Bax., previously shown to well reflect the extent of cell apoptosis in HCC (Duan et al., 2005). Among the compounds tested, TCDD, endosulfan and p,p'DDE showed an anti-apoptotic tendency at 4 h, while hydroquinone induced a strong variation of the apoptotic pattern at 48 h (Fig. 7C and D). At 48 h, TCDD, carbaryl and p,p'DDE displayed pro-apoptotic activity (Fig. 7D). We decided to illustrate the apoptotic dysregulation potentially induced by the chemicals by monitoring the modulation of two caspase inhibitors, the

proteins XIAP (Fig. 7B) and survivin (data not shown). While we detected no modulation of *survivin* gene expression, that of *XIAP*, an anti-apoptotic gene and also a HCC marker associated with a higher metastatic potential and cancer recurrence in patients did change. We only noted an increase in the XIAP gene expression at 48 h when HepG2 cells were treated with endosulfan and carbendazim. Interestingly, neither of these two pesticides showed dysregulation of the apoptotic balance at this time point.

3.5. Early modulation of transduction signals

Our investigations then concerned the involvement of the major signaling pathways potentially associated with hepatic dysregulations in response to xenobiotics. Pathways chosen have already demonstrated involvement in angiogenesis, inflammation, proliferation, survival or differentiation processes leading to tumor progression and metastasis. We treated HepG2 cells for 4 h and 48 h and looked for any of the responses generally observed early in the Erk, Akt, Smads and Stat3 pathways (Fig. 8A). Only endosulfan induced a transient activation of the Erk pathway at 4 h. Endosulfan as well as carbendazim also induced an increase in Akt phosphorylation on threonine 308. Both pesticides as well as carbaryl activated the TGF- β pathway early through the phosphorylation of Smad1/5 and Smad2. Finally, these three pesticides also activated the inflammatory pathway Stat3 through its phosphorylation on tyrosine 705.

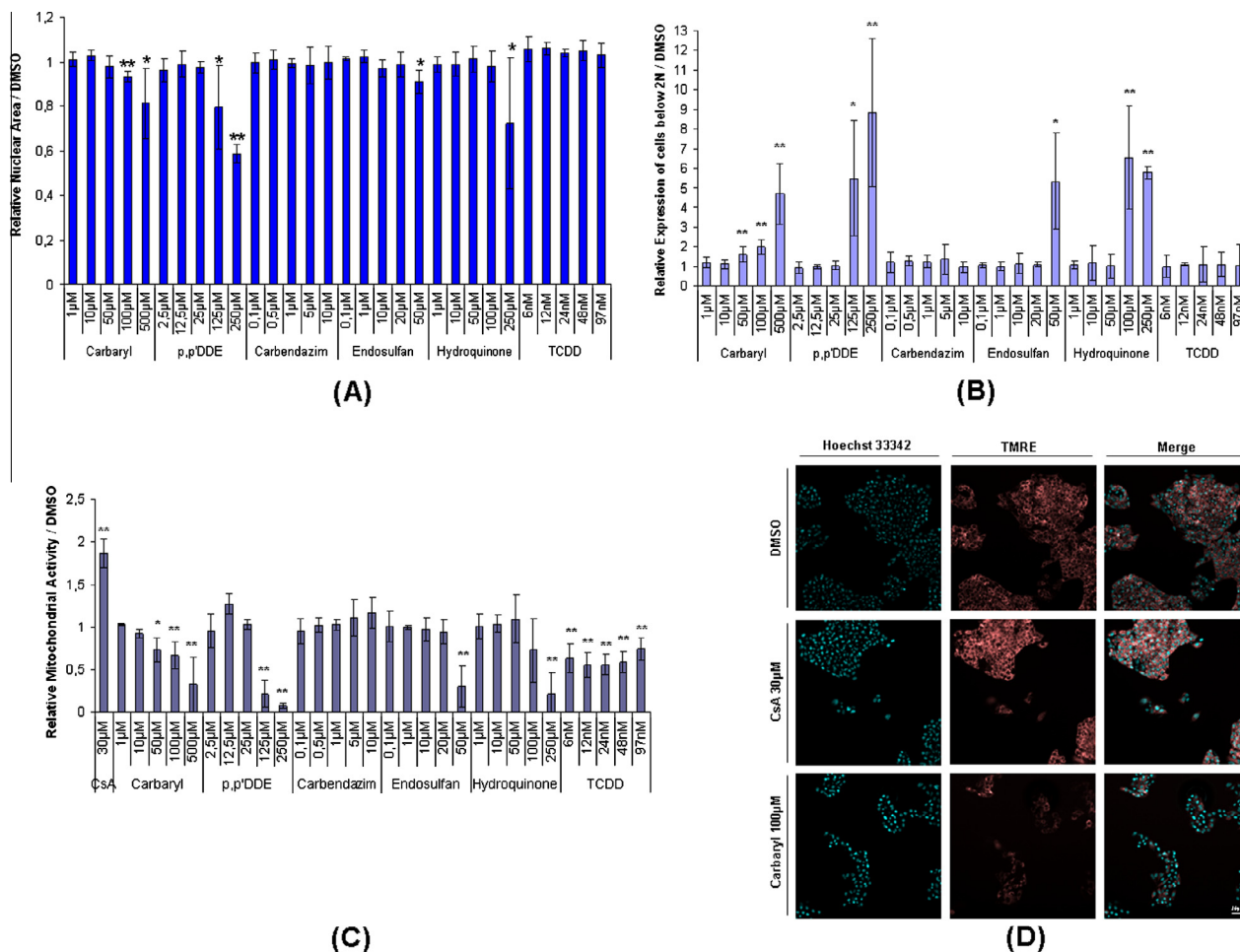


Fig. 4. HCS to complement the viability data. (A, B and C) HepG2 cells were seeded onto 96-well plates and treated with carbaryl (from 1 µM to 500 µM), p,p'DDE (from 2.5 µM to 250 µM), carbendazim (from 0.1 µM to 10 µM), endosulfan (from 0.1 µM to 50 µM), hydroquinone (from 1 µM to 250 µM) or TCDD (from 6 nM to 97 nM). After 24 h treatment, cells were labeled with Hoechst 33342 and tetramethylrhodamine ethyl ester (TMRE) for 30 min before being read on the ArrayScan^{XT1}. (A) Nuclear area was calculated following the 'compartmental' protocol and is based on Hoechst 33342 detection. The relative area was compared to DMSO-treated cells taken as 1. (B) Population of cells below 2N was calculated following the 'cell cycle' protocol and also compared to DMSO-treated cells. (C and D) Mitochondrial activity was calculated using TMRE fluorescence intensity following the 'compartmental' protocol. Cyclosporin A was used as the positive control and was added 30 min before staining. Error bars indicate the mean ± SEM of triplicate determinations in three independent experiments. **P* < 0.05; ***P* < 0.01.

3.6. Effect of xenobiotics on epithelial–mesenchymal transition

Epithelial mesenchymal transition results in a loss of epithelial markers through the activation of specific pathways and transcription factors, and in a gain of mesenchymal characteristics ultimately giving cells the capacity to migrate and invade the surrounding tissue. Firstly quantitative PCR revealed that treatment with TCDD, endosulfan and carbendazim resulted in the downregulation of *CDH1*, a gene coding for the epithelial marker E-cadherin, the main protein of the adherent junctions (Fig. 8B). These three chemicals also induced stabilization of β-catenin (Fig. 8C) in HepG2 cells which was immediately after exposure with endosulfan, early and transient after with carbendazim and later on with dioxin. Finally, we observed an increase of Snail1 protein expression at 4 h after endosulfan treatment (Fig. 8C), a phenomenon that could in part explain the downregulation of *CDH1* gene expression.

Using quantitative PCR, we then observed the modulation of three mesenchymal genes involved in the process of EMT: the *FSP1* gene encoding the clinical marker S100A4 (Fig. 9A), *FN1* gene encoding the extracellular matrix protein fibronectin (Fig. 9B) and *ILK* gene, encoding the integrin-linked kinase which participates in Akt activation through integrin engagement (Fig. 9C). Endosulfan at 24 h (data not shown) and carbendazim at 48 h modulated the

expression of *FSP1*, whereas fibronectin was induced by endosulfan only. Both endosulfan and carbendazim induced an increase in expression of *ILK*. Finally, we investigated whether the compounds could induce the activation of the Fak pathway involved in the EMT process that is essential for cell migration (Fig. 9D and E). To this end, we decided to compare the level of total Fak protein with its phosphorylated form. We observed an increase in activation when HepG2 cells were treated with TCDD and endosulfan whereas p,p'DDE and hydroquinone were associated with low levels of phosphorylation.

3.7. Use of specific pharmacological inhibitors with real-time cellular impedance to target the main pathways responsible for the events engaged in the response to chemicals

Finally, we wished to determine whether the pathways involved in the response to xenobiotic treatment were specific to the impedance profile observed. To this end, we selected endosulfan, TCDD and carbendazim, the three compounds found to activate the major pathways involved in cancer progression and enhance the level of detection of biomarkers of EMT, apoptosis and the cell cycle. We hypothesized that inhibition of the cellular transduction pathways with a specific inhibitor would both disrupt

	Endosulfan						Carbaryl						Carbendazim									
	100nM	1µM	10µM	20µM	50µM	100µM	200µM	1µM	10µM	50µM	100µM	500µM	1mM	5mM	100nM	500nM	2.5µM	5µM	10µM	50µM	125µM	
Cellular impedance	Green	Green	Green	Green	Green	Red	Red	Green	Green	Green	Green	Green	Green	Green	Green	Green	Green	Green	Red	Red	Red	Red
Cell viability	White	White	White	White	White	Red	Red	White	White	White	White	White	White	White	White	White	White	White	Red	Red	Red	Red
Nuclear integrity	White	White	White	White	White	NT	NT	White	White	White	White	White	White	White	White	White	White	White	White	White	NT	NT
Mitochondrial activity	White	White	White	White	White	NT	NT	White	White	White	White	White	White	White	White	White	White	White	White	White	NT	NT

	p,p'DDE						Hydroquinone						TCDD									
	2.5µM	12.5µM	25µM	125µM	250µM	625µM	1,25mM	1µM	10µM	50µM	100µM	250µM	500µM	1mM	6nM	12nM	24nM	48nM	97nM	194nM	387nM	
Cellular impedance	Green	Green	Green	Red	Red	Red	Red	White	Green													
Cell viability	White	White	White	Red	Red	Red	Red	White														
Nuclear integrity	White	White	White	Red	Red	NT	NT	White	NT	NT												
Mitochondrial activity	White	White	White	Red	Red	NT	NT	White	NT	NT												

Area of interest

 No modulation

NT

Fig. 5. A summary of the modulations observed in response to the 6 compounds tested. A subtoxic zone called “zone of interest” has been selected based on various parameters set.

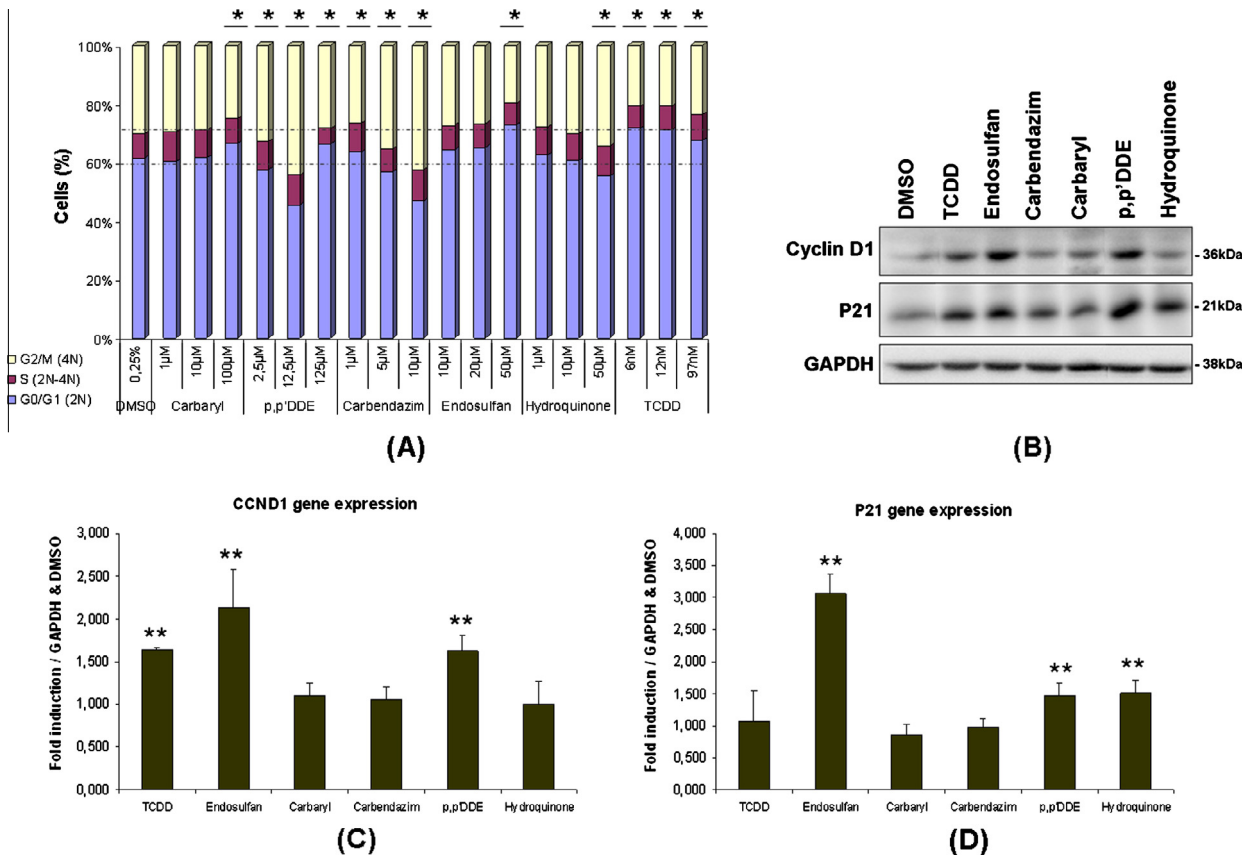


Fig. 6. Effects of the environmental pollutants on the cell cycle. (A) HepG2 cells were seeded onto 96-well plates and treated for 24 h with carbaryl (1, 10 and 100 µM), p,p'DDE (2.5, 12.5 and 125 µM), carbendazim (1, 5 and 10 µM), endosulfan (10, 20 and 50 µM), hydroquinone (1, 10 and 50 µM) or TCDD (6, 12 and 97 nM). Cells were stained with Hoechst 33342 for 30 min and the percentage of cells in each phase was calculated following the ArrayScan^{XTI} 'cell cycle' protocol. (B) HepG2 cells were treated with 10 nM TCDD, 20 µM endosulfan, 10 µM carbaryl, 2.5 µM carbendazim, 5 µM p,p'DDE or 10 µM hydroquinone for 48 h. Cells were lysed and cyclin D1 and P21^{wa1} protein levels were assessed by western blotting. (C and D) *CCND1* and *P21* mRNA levels were assessed by real-time RT-PCR after 48 h treatment with each compound. For all experiments, relative mRNA levels with respect to *GAPDH* mRNA levels are given, and the mRNA levels in DMSO-treated cells are taken as 1. Error bars indicate the mean ± SEM of triplicate determinations in three independent experiments. **P* < 0.05; ***P* < 0.01.

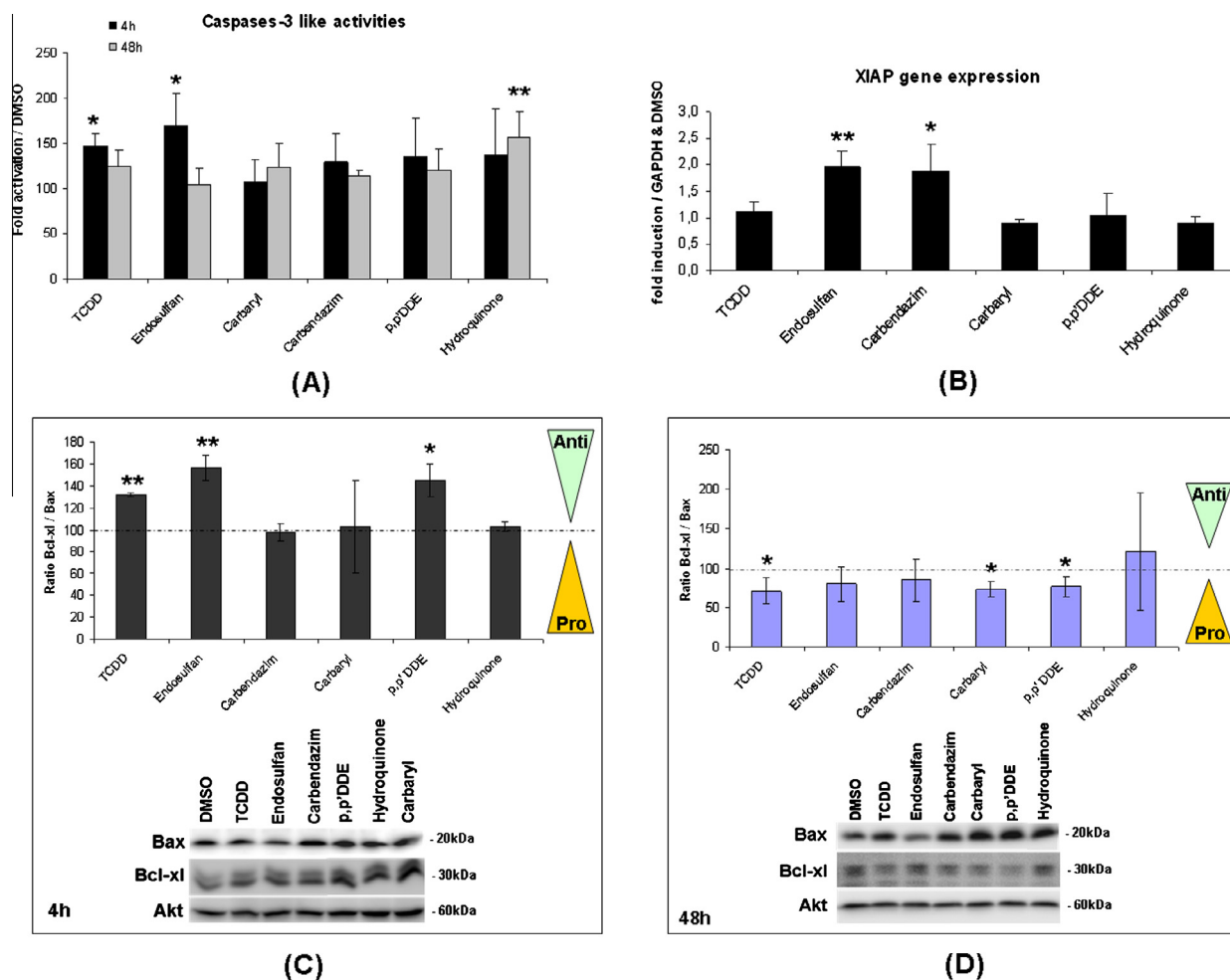


Fig. 7. Dysregulation of the apoptotic pathway. (A) HepG2 cells were treated with 10 nM TCDD, 20 μ M endosulfan, 10 μ M carbaryl, 2.5 μ M carbendazim, 5 μ M p,p'DDE or 10 μ M hydroquinone for 48 h. The cells were then lysed and caspase-3 activity assayed. Results are expressed as a percentage of DMSO-treated cells, designated as 100%. Data are means \pm SD of four independent experiments (note: * $P < 0.05$, ** $P < 0.001$). (B) XIAP mRNA levels were assessed by real-time RT-PCR after 48 h treatment with each compound. For all real-time RT-PCR experiments, relative mRNA levels with respect to GAPDH mRNA levels are given, and the mRNA levels in DMSO-treated cells are taken as 1. Error bars indicate the mean \pm SEM of triplicate determinations in three independent experiments. * $P < 0.05$; ** $P < 0.01$. (C and D) HepG2 cells were treated with the same concentration of chemicals as outlined above, for 4 and 48 h. Bcl-xl and Bax protein levels were evaluated by western blot analysis. Akt protein detection was included as a control for equal loading and membrane transfer. Chemiluminescence was quantified after image acquisition with a CCD camera and the ratios obtained (means \pm SD for three independent experiments). The Bcl-xl/Bax ratio was calculated from band densitometry measured in three independent experiments (means \pm S.D. for three experiments) after normalization against the value of DMSO-control cell and Akt (Note: * $P < 0.05$, ** $P < 0.001$).

the cell impedance profile and block the dependent modulations of associated markers. We detected no effect during the first 48 h of treatment on the HepG2 cells of the inhibitors of the ERK/MEK pathway (5 μ M U0126), the PI3 K/AKT pathway (10 μ M LY294002) or the TGF- β pathway (10 μ M SB431542) at the specified concentrations (data not shown). We focused on the ERK pathway because the U0126 was the only pharmacological inhibitor able to disrupt the TCDD and endosulfan impedance profiles of HepG2 (Fig. 10A and C); no effect on impedance profiles was detected following co-treatment with carbendazim and any of the three inhibitors (data not shown). Although we were unable to detect Erk1/2 phosphorylation after TCDD treatment, the real-time cellular impedance disruption under the influence of the ERK inhibitor allowed us to confirm the possible involvement of the MAPK/ERK pathway in response to TCDD on HepG2 cells, in agreement with that described in the literature (Pierre et al., 2011). Supplementary data show that the U0126 prevented the upregulation of the *CCND1* gene, a well known target of the Erk1/2 pathway but also a HCC prognosis marker, induced by TCDD and endosulfan (Fig. 10B and D). These data suggest that TCDD and endosulfan-induced deregulation of *CCND1* expression should

be Erk1/2 dependent. Aiming to confirm this, we tested whether the EMT induction observed on HepG2 cells in response to these two chemicals was governed by the same pathway. Supplementary qPCR on different EMT markers used in Figs. 7 and 8 failed to confirm this phenomenon and instead supported a more a pro-epithelial effect of the inhibitor U0126 in increasing the transcription basal level of epithelial genes (*CDH1*) and in decreasing drastically the mesenchymal ones (*ILK*, *FN1*; data not shown).

4. Discussion

Here we have described the first combined approach using EMT biomarkers, apoptotic proteins, cell cycle regulators, High Content Screening (HCS) and real-time cellular impedance monitoring technology to investigate the *in vitro* pro-carcinogenic effects of xenobiotics at non toxic doses. Our aim was to assess six environmental pollutants and to detect events which could predict tumor promotion towards metastasis. We used cellular impedance as an indicator of cellular and morphologic changes in response to six compounds. We also chose a range of EMT biomarkers commonly

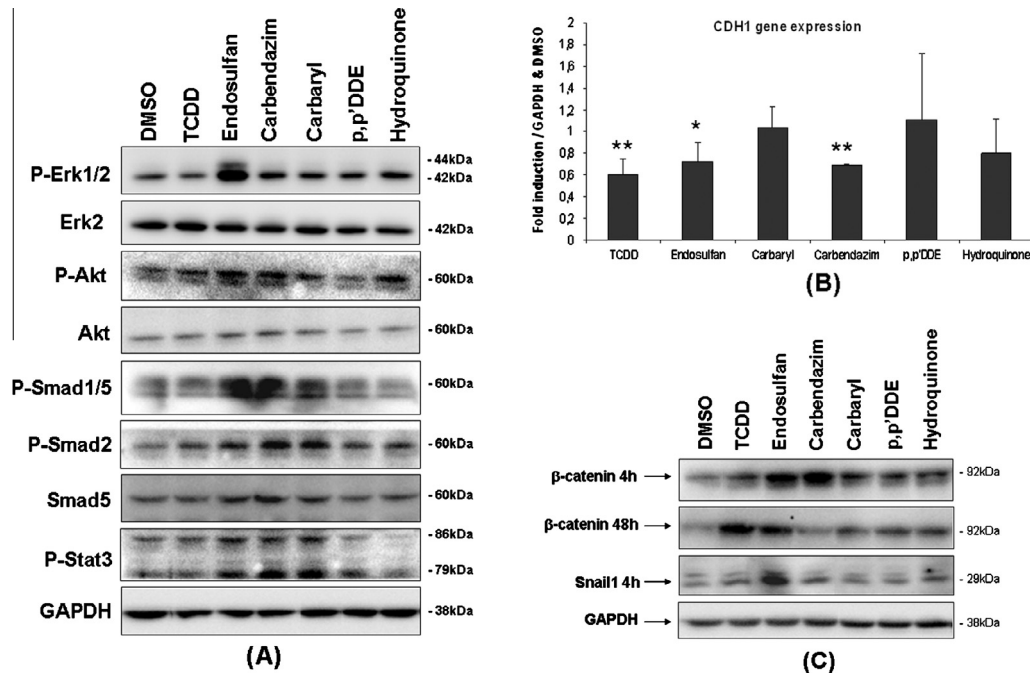


Fig. 8. Early modulation of transduction signals. (A) HepG2 cells were exposed to 10 nM TCDD, 20 μ M endosulfan, 2.5 μ M carbendazim, 10 μ M carbaryl, 5 μ M p,p'DDE or 10 μ M hydroquinone. After 4 h of treatment, cells were lysed and subjected to western blotting, as described in Materials and Methods. Signaling pathways were studied by analyzing the levels of respectively phospho-ERK1/2 and total Erk2 for the ERK1/2 pathway, phospho- and total Akt for the AKT/PI3 K pathway, phospho-Smad1/2/5 and total Smad5 for the TGF- β pathway, and phospho-Stat3 for the STAT pathway. As a control, the same membranes were also probed with an antibody directed against GAPDH. (B) CDH1 mRNA levels were assessed by real-time RT-PCR after 48 h treatment with each compound. For all real-time RT-PCR experiments, relative mRNA levels with respect to GAPDH mRNA levels are given and the mRNA levels in DMSO-treated cells are taken as 1. Error bars indicate the mean \pm SEM of triplicate determinations in three independent experiments. * P < 0.05; ** P < 0.01. (C) Cells were treated as outlined above for 4 h or 48 h. They were then lysed and β -catenin and Snail1 protein levels were assessed by western blotting (results representative of three experiments). As a control, the same membranes were also probed with an antibody directed against GAPDH.

used in HCC and corroborating *in vitro* cell culture. To further validate our findings we studied cell cycle regulators (P21^{waf1} and cyclin D1), early pathway activations (ERK, AKT, SMAD1/2/5 and STAT3), caspase-3 activity and pro- and anti-apoptotic proteins (Bax, Bcl-xl, and XIAP), known to be deregulated during hepatocarcinogenesis progression. We have summarized and ranked the dysregulations observed in response to the six chemicals used (Fig. 11).

Endosulfan, TCDD and carbendazim were the three pesticides associated with most disturbances of the major cellular processes. Firstly, they all induced downregulation of the epithelial marker CDH1 coding for E-cadherin protein, with stabilization of β -catenin through an increase in its protein expression. Such stabilization can lead to the activation of the Wnt/ β -catenin pathway and play an additional role in tumorigenesis should it cooperate with other signaling pathways (Nejak-Bowen and Monga, 2011). Among all the repressor factors known to repress E-cadherin gene expression, we focused on Snail1 and observed its early up-regulation after endosulfan treatment, suggesting that other repressors or a later Snail1 activation could be involved in CDH1 down-regulation after TCDD and carbendazim exposure. In parallel, endosulfan, TCDD and carbendazim also modulated the gene expression of different mesenchymal markers such as fibronectin, with endosulfan, or S100a4 and ILK, with both carbendazim and endosulfan. In contrast, p,p'DDE, carbaryl and hydroquinone treatment produced no detectable modulations in the expression of the EMT biomarkers. The increase in S100a4 (encoded by FSP1) observed following treatment with xenobiotics may be relevant with regards to liver cancer progression. Indeed S100a4 is implicated in many processes including differentiation and inflammation and its expression is strongly associated with metastasis (Garrett et al., 2006; Liu et al., 2013). Moreover, ILK, the expression of which is also increased by

endosulfan and carbendazim, is a key player in integrin-mediated signal transduction. It dependently or independently of FAK contributes towards resistance of anoikis, an apoptosis phenomenon consecutive to loss of adherent junctions that occurs during cancer progression (Paoli et al., 2013). Interestingly, FAK was found strongly activated after TCDD exposure whereas p,p'DDE led to a reduction in the basal phosphorylation level indicating the likely presence of poor adhesion. Considering the evidence for their induced loss of E-cadherin, gain of mesenchymal markers and activation of the ILK or/and Fak pathway, endosulfan, TCDD and carbendazim appear to be EMT process inducers.

Among all the compounds tested, only endosulfan and carbendazim seemed to be able to rapidly activate most of the pathways studied. Interestingly, endosulfan showed a parallel activation of both ERK and SMAD pathways. The cooperation between MAPK and TGF- β has been shown to be crucial for EMT induction and hepatocyte survival (Fischer et al., 2005). Concerning carbendazim and carbaryl, the activation of the SMAD pathway on such cancer cells can be linked to the deregulation of homeostasis and the promotion of cancer progression through EMT induction (Jain et al., 2010). We also noted that endosulfan, carbendazim and carbaryl were able to activate, in parallel to SMAD, the Stat3 pathway involved in the production of cytokines responsible for tumor maintenance and progression (Subramaniam et al., 2013). This phenomenon has already been described in HepG2 cells and in mouse primary hepatocytes, and is associated with chronic inflammation (Besson-Fournier et al., 2012). Finally, endosulfan and carbendazim increased the level of Akt phosphorylation which could impact on many processes but in particular here may be directly linked with EMT and cell survival.

With regards resistance to apoptosis, TCDD and endosulfan showed an early anti-apoptotic profile with the change in Bax/

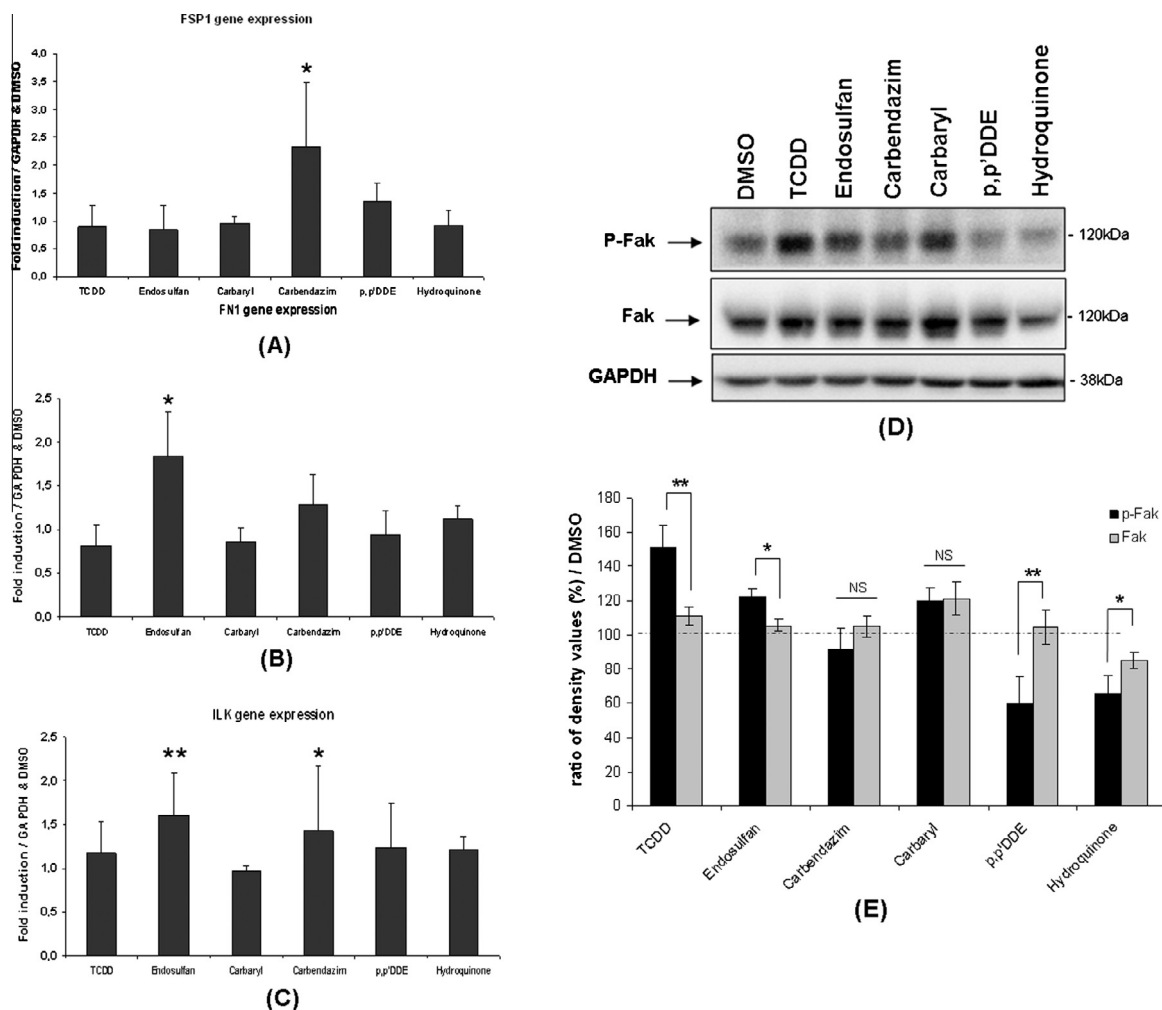


Fig. 9. Effect of xenobiotics on epithelial-mesenchymal transition. (A, B and C) HepG2 cells were treated with 10 nM TCDD, 20 μ M endosulfan, 10 μ M carbaryl, 2.5 μ M carbendazim, 5 μ M p,p'DDE or 10 μ M hydroquinone. *FSP1*, *FN1* and *ILK* mRNA levels were assessed by real-time RT-PCR after 48 h of treatment. For all real-time RT-PCR experiments relative mRNA levels with respect to *GAPDH* mRNA levels are given, and the mRNA levels in DMSO-treated cells are taken as 1. Error bars indicate the mean \pm SEM of triplicate determinations in three independent experiments. * $P < 0.05$; ** $P < 0.01$. (D) Cells were treated as described above for 4 h. They were lysed and Fak and its phosphorylated form p-Fak protein levels were assessed by western blotting (results representative of three experiments). As a control, the same membranes were also probed with an antibody directed against GAPDH. (E) Band densitometry corresponding to immunoblots shown in (D) was performed after the acquisition with a CCD camera. The results are defined as the ratio between treated cells versus DMSO-treated cells normalized by GAPDH (means \pm S.D. for three experiments).

Bcl-xl balance. Yet, the increase in caspase-3 activity observed is normally consecutive to the induction of an apoptotic process. This phenomenon has already been described by our team (Peyre et al., 2012) and is linked to an anoikis process. The number of modulations and near-identical behavior observed between dioxin and endosulfan, would indicate the same mechanism of action between the two pesticides. This phenomenon tends to be abrogated at 48 h after endosulfan exposure with in particular the increase in *XIAP* gene expression. It also occurs after carbendazim treatment and is correlated in HCC cells with metastasis and resistance to apoptosis (Shi et al., 2008). XIAP also inhibits caspase activity, which in part could explain the absence of apoptosis at 48 h after treatment with endosulfan. At this point, both carbaryl and p,p'DDE induce a low change in the apoptotic balance leading to a pro-apoptotic response whereas hydroquinone treatment is followed by an increase in caspase-3 activity without a well-defined dysregulation in Bcl-xl/Bax balance (high variability observed).

With regards the cell cycle, we observed that p,p'DDE acts as a proliferator through MTT results (120–130% of viability compared to the DMSO control between 2.5 and 25 μ M), impedance positive curves which perfectly matched the viability test, cell cycle assay which highlighted the increase in the G2/M phase, and through

the increase in *CCND1* both at the gene and protein level. The decrease in the G2/M phase and increase of P21 protein expression induced by TCDD reflects cell cycle arrest in accordance with previous studies (Puga et al., 2000). The increase of *CCND1* gene and protein expression is probably associated with the activation of the Wnt/ β -catenin pathway as observed with endosulfan. The positive curves we observed via real-time cellular impedance together with the EMT responses could be linked to the cell plasticity and migration induced by TCDD on HepG2 cells as previously proposed (Diry et al., 2006). While hydroquinone seems to induce a later stress leading to initiation of an apoptotic cascade and the modulation of P21 gene expression, exposure to endosulfan or TCDD induces similar effects with a possible tendency to cell cycle arrest through high expression of P21^{waf1} (the decrease in the G2/M phase is significant after 50 μ M of treatment).

Using real-time cellular impedance technology (xCELLigence, Roche), we were able to add pertinent data to our common protocol. This innovative approach enhances the sensitivity of detection and could represent a decisive tool for future toxicological investigations when combined with such EMT relevant biomarkers. Among the six chemicals tested, we choose two for the final tests of our investigation. While endosulfan was banned in Europe, little

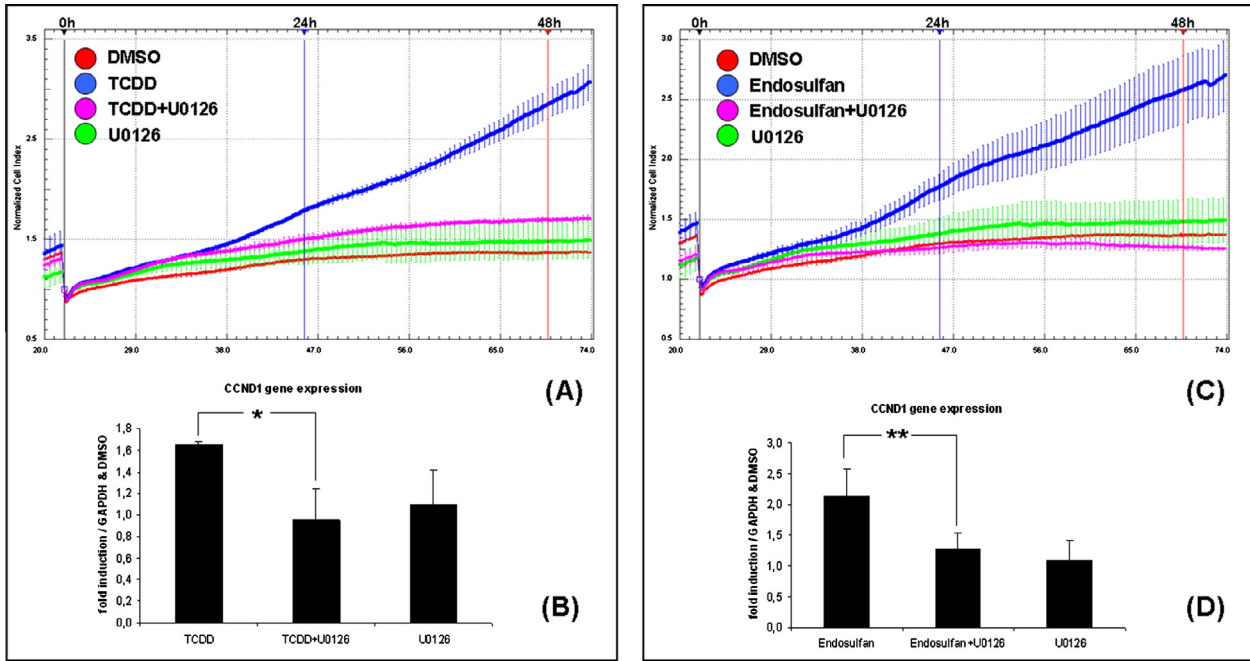


Fig. 10. Use of specific pharmacological inhibitors with real-time cellular impedance to target the main pathways responsible for the events engaged in the response to chemicals. (A and C) HepG2 cells were treated for 48 h with 10 nM TCDD or 20 μM endosulfan with or without 5 μM of U0126. Then, the real-time cellular impedance signatures were obtained using xCELLigence® technology. (B and D) *CCND1* mRNA levels were assessed by real-time RT-PCR after 48 h of treatment, with or without 5 μM of U0126. For all real-time RT-PCR experiments, relative mRNA levels with respect to *GAPDH* mRNA levels are given, and the mRNA levels in DMSO-treated cells are taken as 1. Error bars indicate the mean ± SEM of triplicate determinations in three independent experiments. **P* < 0.05; ***P* < 0.01.

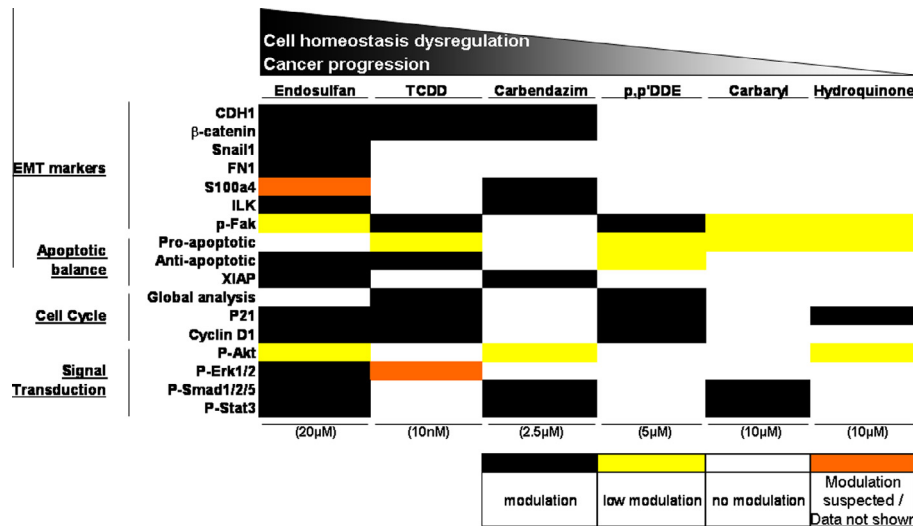


Fig. 11. A summary of the modulations observed in response to the 6 compounds tested. Chemicals have been classified in order of extent of deregulation observed and thus also in order of their carcinogenic potential.

information actually exists concerning its implication in cancer development. Similarly, TCDD has been classified as a class 1 carcinogen by the International Agency for Research on Cancer (IARC), and yet doubt remains over its effects on human health, in particular since it shows opposite effects depending on its concentration and most of the studies and available data are based on animal experiments (Popp et al., 2006; Steenland et al., 2004). Here we attempted to provide new evidence concerning endosulfan and TCDD on the risk of cancer aggravation. The U0126-induced inhibition of NCI when HepG2 cells are treated with TCDD or endosulfan showed a possible involvement of the Erk1/2 pathway in the EMT process. However, we were not able to detect phosphorylation of

the Erk1/2 proteins at 4 h when HepG2 cells were treated with TCDD. Nevertheless, 25 nM TCDD was shown to stimulate Ras activity and ERK1/2 phosphorylation through the induction of SOS1 (Pierre et al., 2011). One explanation for this discrepancy could therefore be that the activation of the ERK pathway brought about by the lower concentration of TCDD (10 nM) used in our experiments fell below the limit of detection. The concentration used was however sufficient to modulate the Erk1/2-dependant cellular impedance profile and in parallel induce the Erk1/2-dependant overexpression of *CCND1*. The link between Erk1/2 pathway and the regulation of *CCND1* gene expression has already been shown (Jin et al., 2011). We can confirm that TCDD and

endosulfan are two chemicals able to modulate the *CCND1* gene expression through the activation of the ERK/MAPK pathway.

To conclude, we have highlighted the pro-carcinogenic effects of endosulfan, TCDD and carbendazim by demonstrating the dysregulation of the TGF- β pathway through Smads activation and possible β -catenin activation. These two events in HCC could together lead to the induction of EMT and cancer cell survival (Fabregat, 2009). Secondly, the phosphorylation of STAT-3 and AKT after treatment with endosulfan and carbendazim is evidence in favor of a conferred resistance to apoptosis, an event associated with the development and progression of tumors in the liver (Fabregat et al., 2007). Thirdly, the induction of caspase activity and the modulation of the expression of apoptotic proteins (XIAP, Bcl-xl, Bax) is further evidence allowing us to reasonably presume that these chemicals can alter the function of apoptosis and contribute to resistance to chemotherapy. All three compounds confer a higher carcinogenic potential to HepG2 cells. Endosulfan, TCDD and p,p'DDE also increase cyclin D1 protein expression. This cell cycle regulator correlates with tumor relapse and is an independent predictive marker for recurrence and prognosis of HCC (Qin and Tang, 2004). Altogether, the numerous pieces of evidence we have gathered here strongly support the occurrence of pro-carcinogenic effects following chronic exposure to chemicals, in particular endosulfan, TCDD and carbendazim, able to induce EMT. We conclude that the combined use of all these biomarkers with real-time cellular impedance and HCS represents a reliable and realistic approach to determine the impact of xenobiotics on liver. The next step towards greater clinical relevance will aim to add to this protocol, any markers of stem cells, inflammation, stress oxidation and hypoxia. Using this *in vitro* approach, further investigations on the deregulation of key hepatic functions, by food or environmental contaminants, could then be conducted.

Funding

The project received a Public Institutional Funding from INRA. This work was also funded by the French Ministry of Ecology (in the frame of the ACTIVISME project) and by the “Conseil Général des Alpes Maritimes” (in the frame of the HCSTOX project).

Conflict of Interest

The authors declare that there are no conflicts of interest.

Transparency Document

The [Transparency document](#) associated with this article can be found in the online version.

Acknowledgments

The authors wish to thank Roche for their help using the real-time cellular impedance technology (xCELLigence®), Jean-Michel Linget, Guy Bouvier and Nicolas Orsini of Galderma R&D for their contribution to this work.

References

ANSES, 2011. Etude de l'alimentation totale française (EAT2). anses.fr/Documents/PASER2006sa0361Ra1.pdf, anses.fr/Documents/PASER2006sa0361Ra2.pdf.

Atienza, J.M., Yu, N., Wang, X., Xu, X., Abassi, Y., 2006. Label-free and real-time cell-based kinase assay for screening selective and potent receptor tyrosine kinase inhibitors using microelectronic sensor array. *J. Biomol. Screen.* 11 (6), 634–643. <http://dx.doi.org/10.1177/1087057106289334>.

Atienzar, F.A., Tilmant, K., Gerets, H.H., Toussaint, G., Speeckaert, S., Hanon, E., Depelchin, O., Dhalluin, S., 2011. The use of real-time cell analyzer technology in drug discovery: defining optimal cell culture conditions and assay reproducibility with different adherent cellular models. *J. Biomol. Screen.* 16 (6), 575–587. <http://dx.doi.org/10.1177/1087057111402825>.

Besson-Fournier, C., Latour, C., Kautz, L., Bertrand, J., Ganz, T., Roth, M.P., Coppin, H., 2012. Induction of activin B by inflammatory stimuli up-regulates expression of the iron-regulatory peptide hepcidin through Smad1/5/8 signaling. *Blood* 120 (2), 431–439. <http://dx.doi.org/10.1182/blood-2012-02-411470>.

Buitrago-Molina, L.E., Marhenke, S., Longerich, T., Sharma, A.D., Boukouris, A.E., Geffers, R., Guigas, B., Manns, M.P., Vogel, A., 2013. The degree of liver injury determines the role of p21 in liver regeneration and hepatocarcinogenesis in mice. *Hepatology* (Baltimore, Md.) 58(3), pp. 1143–1152. <http://dx.doi.org/10.1002/hep.26412>.

Che, Y., Ye, F., Xu, R., Qing, H., Wang, X., Yin, F., Cui, M., Burstein, D., Jiang, B., Zhang, D.Y., 2012. Co-expression of XIAP and cyclin D1 complex correlates with a poor prognosis in patients with hepatocellular carcinoma. *Am. J. Pathol.* 180 (5), 1798–1807. <http://dx.doi.org/10.1016/j.ajpath.2012.01.016>.

Dang, H., Ding, W., Emerson, D., Rountree, C.B., 2011. Snail1 induces epithelial-to-mesenchymal transition and tumor initiating stem cell characteristics. *BMC Cancer* 11, 396. <http://dx.doi.org/10.1186/1471-2407-11-396>.

Diry, M., Tomkiewicz, C., Koehle, C., Coumoul, X., Bock, K.W., Barouki, R., Transy, C., 2006. Activation of the dioxin/aryl hydrocarbon receptor (AhR) modulates cell plasticity through a JNK-dependent mechanism. *Oncogene* 25 (40), 5570–5574. <http://dx.doi.org/10.1038/sj.onc.1209553>.

Duan, X.X., Ou, J.S., Li, Y., Su, J.J., Ou, C., Yang, C., Yue, H.F., Ban, K.C., 2005. Dynamic expression of apoptosis-related genes during development of laboratory hepatocellular carcinoma and its relation to apoptosis. *World J. Gastroenterol.* 11 (30), 4740–4744.

Fabregat, I., 2009. Dysregulation of apoptosis in hepatocellular carcinoma cells. *World J. Gastroenterol.* 15 (5), 513–520.

Fabregat, I., Roncero, C., Fernandez, M., 2007. Survival and apoptosis: a dysregulated balance in liver cancer. *Liver Int.: Official J. Int. Assoc. Study Liver* 27 (2), 155–162. <http://dx.doi.org/10.1111/j.1478-3231.2006.01409.x>.

Fautrel, A., Chesne, C., Guillouzo, A., de Sousa, G., Placidi, M., Rahmani, R., Braut, F., Pichon, J., Hoellinger, H., Vintzou, P., Diarte, I., Melcion, C., Cordier, A., Lorenzon, G., Benicourt, M., Vannier, B., Fournex, R., Peloux, A.F., Bichet, N., Gouy, D., Cano, J.P., Lounes, R., 1991. A multicentre study of acute *in vitro* cytotoxicity in rat liver cells. *Toxicol. In Vitro: Int. J. Publ. Assoc. BIBRA* 5 (5–6), 543–547.

Ferris, I.T.J., Ortega Garcia, J.A., Garcia, I.C.J., Lopez Andreu, J.A., Ribes Koninckx, C., Berbel Tornero, O., 2008. Risks factors for pediatric malignant liver tumors. *Anales de pediatria* (Barcelona, Spain: 2003) 68(4), 377–384. (First published on Factores de riesgo para los tumores hepaticos malignos pediatricos).

Fischer, A.N., Herrera, B., Mikula, M., Proell, V., Fuchs, E., Gotzmann, J., Schulte-Hermann, R., Beug, H., Mikulits, W., 2005. Integration of Ras subeffector signaling in TGF-beta mediated late stage hepatocarcinogenesis. *Carcinogenesis* 26 (5), 931–942. <http://dx.doi.org/10.1093/carcin/bgi043>.

Fuchs, B.C., Fujii, T., Dorfman, J.D., Goodwin, J.M., Zhu, A.X., Lanuti, M., Tanabe, K.K., 2008. Epithelial-to-mesenchymal transition and integrin-linked kinase mediate sensitivity to epidermal growth factor receptor inhibition in human hepatoma cells. *Cancer Res.* 68 (7), 2391–2399. <http://dx.doi.org/10.1158/0008-5472.can-07-2460>.

Garrett, S.C., Varney, K.M., Weber, D.J., Bresnick, A.R., 2006. S100A4, a mediator of metastasis. *J. Biol. Chem.* 281 (2), 677–680. <http://dx.doi.org/10.1074/jbc.R500017200>.

Jain, S., Singhal, S., Lee, P., Xu, R., 2010. Molecular genetics of hepatocellular neoplasia. *Am. J. Trans. Res.* 2 (1), 105–118.

Ji, J., Wang, X.W., 2012. Clinical implications of cancer stem cell biology in hepatocellular carcinoma. *Semin. Oncol.* 39 (4), 461–472. <http://dx.doi.org/10.1053/j.seminoncol.2012.05.011>.

Jin, C., Samuelson, L., Cui, C.B., Sun, Y., Gerber, D.A., 2011. MAPK/ERK and Wnt/beta-Catenin pathways are synergistically involved in proliferation of Sca-1 positive hepatic progenitor cells. *Biochem. Biophys. Res. Commun.* 409 (4), 803–807. <http://dx.doi.org/10.1016/j.bbrc.2011.05.094>.

Ke, N., Wang, X., Xu, X., Abassi, Y.A., 2011. The xCELLigence system for real-time and label-free monitoring of cell viability. *Methods in Molecular Biology* (Clifton, N.J.) 740, pp. 33–43. http://dx.doi.org/10.1007/978-1-61779-108-6_6.

Liu, Z., Liu, H., Pan, H., Du, Q., Liang, J., 2013. Clinicopathological significance of S100A4 expression in human hepatocellular carcinoma. *J. Int. Med. Res.* 41 (2), 457–462. <http://dx.doi.org/10.1177/0300060513478086>.

Mostafalou, S., Abdollahi, M., 2013. Pesticides and human chronic diseases: evidences, mechanisms, and perspectives. *Toxicol. Appl. Pharmacol.* 268 (2), 157–177. <http://dx.doi.org/10.1016/j.taap.2013.01.025>.

Nambotini, S.B., Tomimaru, Y., Merle, P., Wands, J.R., Kim, M., 2012. Functional consequences of WNT3/Frizzled7-mediated signaling in non-transformed hepatic cells. *Oncogenesis* 1, e31. <http://dx.doi.org/10.1038/oncsis.2012.31>.

Nejak-Bowen, K.N., Monga, S.P., 2011. Beta-catenin signaling, liver regeneration and hepatocellular cancer: sorting the good from the bad. *Semin. Cancer Biol.* 21 (1), 44–58. <http://dx.doi.org/10.1016/j.semcancer.2010.12.010>.

O'Brien, P.J., Irwin, W., Diaz, D., Howard-Coffield, E., Krejsa, C.M., Slaughter, M.R., Gao, B., Kaludercic, N., Angeline, A., Bernardi, P., Brain, P., Hougham, C., 2006. High concordance of drug-induced human hepatotoxicity with *in vitro* cytotoxicity measured in a novel cell-based model using high content screening. *Arch. Toxicol.* 80 (9), 580–604. <http://dx.doi.org/10.1007/s00204-006-0091-3>.

- Olson, H., Betton, G., Robinson, D., Thomas, K., Monro, A., Kolaja, G., Lilly, P., Sanders, J., Sipes, G., Bracken, W., Dorato, M., Van Deun, K., Smith, P., Berger, B., Heller, A., 2000. Concordance of the toxicity of pharmaceuticals in humans and in animals. *Regul. Toxicol. Pharmacol.* 32 (1), 56–67.
- Paoli, P., Giannoni, E., Chiarugi, P., 2013. Anoikis molecular pathways and its role in cancer progression. *Biochim. Biophys. Acta.* <http://dx.doi.org/10.1016/j.bbamcr.2013.06.026>.
- Peyre, L., Zucchini-Pascal, N., de Sousa, G., Rahmani, R., 2012. Effects of endosulfan on hepatoma cell adhesion: Epithelial–mesenchymal transition and anoikis resistance. *Toxicology* 300 (1–2), 19–30. <http://dx.doi.org/10.1016/j.tox.2012.05.008>.
- Pierre, S., Bats, A.S., Chevallier, A., Bui, L.C., Ambolet-Camoit, A., Garlatti, M., Aggerbeck, M., Barouki, R., Coumoul, X., 2011. Induction of the Ras activator Son of Sevenless 1 by environmental pollutants mediates their effects on cellular proliferation. *Biochem. Pharmacol.* 81 (2), 304–313. <http://dx.doi.org/10.1016/j.bcp.2010.10.003>.
- Popp, J.A., Crouch, E., McConnell, E.E., 2006. A Weight-of-evidence analysis of the cancer dose-response characteristics of 2,3,7,8-tetrachlorodibenzodioxin (TCDD). *Toxicol. Sci.: Official J. Soc. Toxicol.* 89 (2), 361–369. <http://dx.doi.org/10.1093/toxsci/kfj016>.
- Puga, A., Maier, A., Medvedovic, M., 2000. The transcriptional signature of dioxin in human hepatoma HepG2 cells. *Biochem. Pharmacol.* 60 (8), 1129–1142.
- Qin, L.X., Tang, Z.Y., 2004. Recent progress in predictive biomarkers for metastatic recurrence of human hepatocellular carcinoma: a review of the literature. *J. Cancer Res. Clin. Oncol.* 130 (9), 497–513. <http://dx.doi.org/10.1007/s00432-004-0572-9>.
- Shi, Y.H., Ding, W.X., Zhou, J., He, J.Y., Xu, Y., Gambotto, A.A., Rabinowich, H., Fan, J., Yin, X.M., 2008. Expression of X-linked inhibitor-of-apoptosis protein in hepatocellular carcinoma promotes metastasis and tumor recurrence. *Hepatology* (Baltimore, Md.) 48(2), pp. 497–507. <http://dx.doi.org/10.1002/hep.22393>.
- Steenland, K., Bertazzi, P., Baccarelli, A., Kogevinas, M., 2004. Dioxin revisited: developments since the 1997 IARC classification of dioxin as a human carcinogen. *Environ. Health Perspect.* 112 (13), 1265–1268.
- Subramaniam, A., Shanmugam, M.K., Perumal, E., Li, F., Nachiyappan, A., Dai, X., Swamy, S.N., Ahn, K.S., Kumar, A.P., Tan, B.K., Hui, K.M., Sethi, G., 2013. Potential role of signal transducer and activator of transcription (STAT)3 signaling pathway in inflammation, survival, proliferation and invasion of hepatocellular carcinoma. *Biochim. Biophys. Acta* 1835 (1), 46–60. <http://dx.doi.org/10.1016/j.bbcan.2012.10.002>.
- Tolosa, L., Pinto, S., Donato, M.T., Lahoz, A., Castell, J.V., O'Connor, J.E., Gomez-Lechon, M.J., 2012. Development of a multiparametric cell-based protocol to screen and classify the hepatotoxicity potential of drugs. *Toxicol. Sci.: Official J. Soc. Toxicol.* 127 (1), 187–198. <http://dx.doi.org/10.1093/toxsci/kfs083>.
- Xu, J.J., Henstock, P.V., Dunn, M.C., Smith, A.R., Chabot, J.R., de Graaf, D., 2008. Cellular imaging predictions of clinical drug-induced liver injury. *Toxicol. Sci.: Official J. Soc. Toxicol.* 105 (1), 97–105. <http://dx.doi.org/10.1093/toxsci/kfn109>.
- Yang, J.D., Nakamura, I., Roberts, L.R., 2011. The tumor microenvironment in hepatocellular carcinoma: current status and therapeutic targets. *Semin. Cancer Biol.* 21 (1), 35–43. <http://dx.doi.org/10.1016/j.semcancer.2010.10.007>.
- Zucchini-Pascal, N., Peyre, L., Rahmani, R., 2013. Crosstalk between beta-catenin and snail in the induction of epithelial to mesenchymal transition in hepatocarcinoma: role of the ERK1/2 pathway. *Int. J. Mol. Sci.* 14 (10), 20768–20792. <http://dx.doi.org/10.3390/ijms141020768>.